The preparation by true liquid crystal templating of mesoporous silicates containing nanoparticulate metals†

Nicola C. King,‡[a] Ross A. Blackley,[b] Wuzong Zhou[b] and Duncan W. Bruce*[c]

Received (in Cambridge, UK) 26th May 2006, Accepted 12th June 2006
First published as an Advance Article on the web 3rd July 2006
DOI: 10.1039/b607470g

Mesostructured silicates containing metal nanoparticles have been synthesised *via* templating around a pre-formed, metal-containing mesophase using a non-ionic surfactant.

Since the discovery of the M41S silicates,[1] there has been an enormous expansion in the field of mesoporous molecular sieves and in particular in the incorporation of metals within the silicate and the subsequent enhancement of silicate functionality. Particular emphasis has been placed on the post-synthetic introduction of both metal complexes and nanoparticles into pre-formed silicates; such nanoparticles can be imaged directly by TEM.[2]

In the original syntheses, pore morphology cannot be predicted *a priori*, even though a given reaction protocol is reproducible. However, Attard *et al.*[3] showed how pre-formed liquid crystal mesophases of neutral and cationic surfactants could be used to template silicates using a sol–gel methodology and how the pore morphology of the final silicate was pre-determined by the structure of the liquid crystal phase on which it was templated. This was termed True Liquid Crystal Templating (TLCT).

In seeking new routes to mesoporous silicates containing metal or metal oxide particles, we used the hexagonal H_1 mesophase[4] of some Ru^{II}–bipyridine surfactants.[5] Using true liquid crystal templating, we prepared mesostructured silicates doped with RuO_2[6] which were effective catalysts for alkene hydrogenation[7] and water oxidation.[8]

Attractive as such an approach is, our work has shown that finding other metallosurfactants that act in such a well-behaved manner is fraught with difficulty; clearly, another approach is required.

Dag *et al.* showed that lyotropic mesophases of non-ionic surfactants containing the nitrate salts of hexaaqua metal cations, $[M(OH_2)_6](NO_3)_2$, can be prepared both in the presence and absence of uncoordinated water,[9] and it was also shown that Au and Pt may be incorporated by adding $H[AuCl_4]$ or $H_2[PtCl_6]$ to the aqueous mesophase of an ethylene oxide surfactant prior to sol–gel condensation.[10] However the resulting materials had a poorly defined structure and were unstable mechanically, likely due to the strongly acidic medium in which condensation occurred, leading to rapid condensation.

We now report that by using Group 1 metal salts of either commercial chlorometallate anions of heavier transition metals or of anionic EDTA complexes, we can flexibly access a range of metal-containing, mesoporous silicates of well-defined structure with high surface areas and thick pore walls.

Thus, a 50 wt% mixture of polyoxyethylene-10-lauryl ether ($C_{12}EO_8$) in water exists in the hexagonal H_1 phase at room temperature. The salts $K[AuCl_4]$, $K_2[PdCl_4]$, $K_2[PtCl_4]$ and $Na_3[IrCl_6]$ were dissolved in water (10 wt%, pH ~ 2 with HCl) and mixed with $C_{12}EO_8$ (1 : 1); the resulting mixtures were observed also to be in the H_1 phase. The mesophases formed were then employed in the TLCT synthesis of mesoporous silicates and, after condensation at room temperature for 48 h, the silicate was calcined by heating to 400 °C at 3 K min^{-1} under N_2 and holding there in air for 5 h, before cooling to room temperature.

However, the related halometallate anions of first-row transition metals hydrolyse immediately to give, we presume, the hexaaqua complex, which proved an unsuitable co-component for templating. Therefore, to retain the analogy with the noble metal salts, we sought other ligands for the metals that, when complexed, would generate an anionic complex that would be sufficiently inert to resist hydrolysis. We therefore selected EDTA. Thus, the salts Na[M(EDTA)] (M = Fe, Co and Cr) were obtained and silicates were prepared exactly as described for the halometallate anions.

For all silicates, as-synthesised and calcined materials were characterised by low-angle X-ray scattering and the calcined material was also subject to analysis by BET-N_2 sorption, TEM and XPS. The pore characteristics of the materials synthesised are given in Table 1 and are compared to those typical for the blank silicate.

Table 1 shows that the materials possess very similar pore characteristics (pore diameters obtained using the EDTA complexes were slightly lower) although there is a slight decrease in surface area upon metal incorporation. This is unsurprising since the pores are partially filled with metal nanoparticles; such effects have been remarked on previously.[11] All N_2-sorption isotherms obtained were type IV and showed no hysteresis, indicative of a narrow pore size distribution.

The low-angle XRD pattern shown in Fig. 1 was obtained for the Pd-containing silicate and is typical of all the materials synthesised – another example is found in the ESI.† The three peaks observed for the calcined material can be indexed to the d_{10}, d_{11} and d_{20} reflections of a two-dimensional, hexagonal unit cell. Whilst there is only one diffraction peak from the as-synthesised material (prior to calcination), it can be assumed that this is the d_{10} of a hexagonal unit cell since polarising optical microscopy shows an optical texture typical of the hexagonal H_1 mesophase. There is a shift to higher values of 2θ upon calcination corresponding to a

[a]*Department of Chemistry, University of Exeter, Stocker Road, Exeter, UK EX4 4QD*
[b]*School of Chemistry, University of St Andrews, St Andrews, UK KY16 9ST*
[c]*Department of Chemistry, University of York, Heslington, York, UK YO10 5DD. E-mail: db519@york.ac.uk; Fax: +44 1904 432516; Tel: +44 1904 434085*
† Electronic supplementary information (ESI) available: TEM image; ^{29}Si MAS-NMR spectra. See DOI: 10.1039/b607470g
‡ *Present address*: School of Biosciences, Geoffrey Pope Building, University of Exeter, Stocker Road, Exeter, UK EX4 4QD.

Table 1 Structural data for metal-containing mesoporous silicates

Metal	Loading[a]/wt%	Surface area/m^2 g^{-1}	*d*-spacing/Å	Lattice parameter/Å	Pore diameter/Å	Pore wall thickness[b]/Å
—	—	947	38.7	44.7	26.9	17.8
Pd	5.6	908	39.8	46.0	27.5	18.5
Au	6.0	710	41.2	47.6	28.1	19.5
Ir	4.6	748	39.6	45.6	26.2	19.4
Pt	1.6[c]	838	39.8	46.0	26.5	19.6
Fe	2.0	819	38.2	44.1	23.3	20.8
Co	2.0	1111	41.7	48.2	25.1	20.1
Cr	1.7	802	37.6	43.4	21.5	16.1

[a] Metal loading in calcined silicate, from a synthesis gel in which the aqueous regions are 10 wt% metal precursor. [b] Calculated. [c] Metal loading in calcined silicate, from a synthesis gel in which the aqueous regions are 2.5 wt% metal precursor.

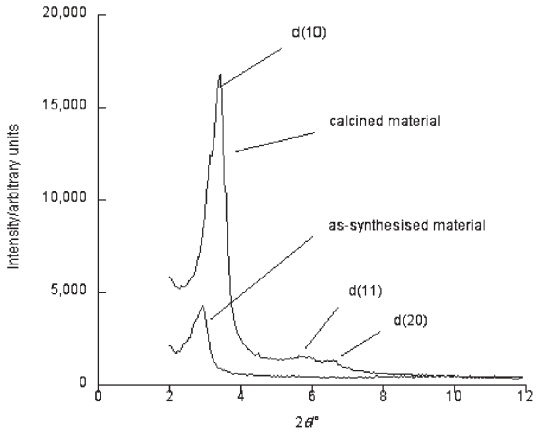

Fig. 1 Low-angle X-ray scattering pattern for Pd-containing silicate.

contraction in the lattice caused by completion of silicate condensation. The increase in intensity of the peaks and subsequent appearance of higher-angle reflections is due to a stiffening of the lattice and increase in overall structural order upon calcination.[12] The hexagonal nature of the silicate and the length of the pores was also confirmed by TEM; 'end-on' and 'side-on' views are shown as Fig. S2.†

Crucial to this synthetic approach is the behaviour of the metals upon calcination. Upon condensation, the materials were observed to retain their colour in the aqueous portion, due to the presence of the metal ion, and their translucency, indicating that the metal complex had not crystallised despite the absense of water. This latter observation we attribute to complexation of the Group 1 metal cation by the ethylene oxide headgroup. Also important here is that the anions are relatively inert under the reaction conditions so that there is little, if any, hydrolysis during condensation, meaning that the metal is not incorporated into the silicate framework.

Upon calcination the silicates changed colour and became opaque. $^{29}Si\{^1H\}$ MAS-NMR spectra (Fig. S3†) showed that the as-synthesised silicate contained a significant quantity of Q_2 silicon sites due to only partial condensation; such materials typically possess limited hydrothermal stability. After calcination, no Q_2 sites were observed and there was a much higher proportion of Q_4 sites (four Si–O–Si linkages) compared to Q_3 (three Si–O–Si plus one Si–OH). Calcination also causes the decomposition of the complex anion and the metal is deposited within the pores as metallic nanoparticles.

From Fig. 2 it is clear to see that the metals do not all behave in the same way. The Pd-containing silicate (Fig. 2a) was found by wide-angle X-ray scattering to contain palladium metal and from the TEM images the particles were found to be approximately 5–6 nm in diameter, that is they aggregate such that they fill two pores. The silicate, which was previously red/brown, became black on calcination. TEM analysis showed that the surface of the Pd-containing material was clean, there were no metal deposits on the surface of the silicate, thus we can conclude that all the metal is retained and deposited as nanoparticles within the pores. A similar observation is made for the Au-containing material (Fig. S4†) although in this image, some of the pore structure of the material has been destroyed during the imaging process. The particles observed are similar in size to the Pd particles, although this cannot easily be observed directly due to beam damage caused to the silicate network. XPS analysis showed the gold to be deposited within the pores as Au^0 and upon calcination, the silicate changed from a translucent yellow colour to red and opaque.

The iridium-containing material, black after calcination, also exhibits a uniform array of particles within the porous structure of the silicate, however the particles are smaller than was observed for Au and Pd and appear to be constrained within single pores, being ~3 nm in diameter (Fig. 2b). However, some deposits of larger particles were also observed on the surface of the silicate, probably due to inhomogenities in sample preparation. Therefore, the

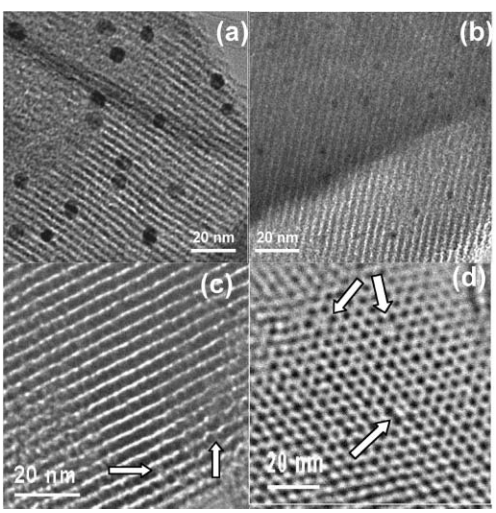

Fig. 2 TEM images of mesoporous silicates containing (a) Pd, (b) Ir; the black dots are metallic nanoparticles inside the pores. (c) Fe-containing sample viewed down the [100] direction. The arrows indicate some Fe nanoparticles inside the channels. (d) Fe-containing sample viewed down the pore axis under an over-focus condition. The arrows show unusual image contrast.

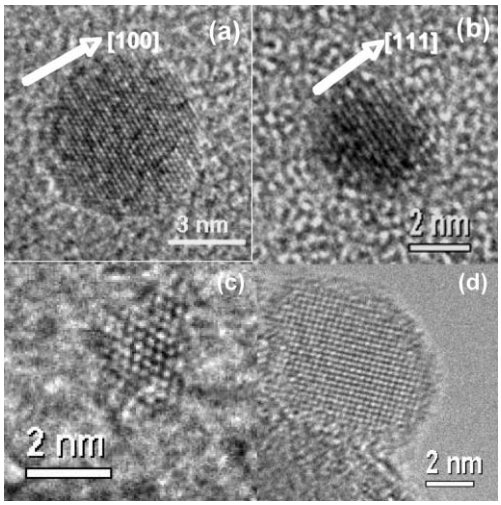

Fig. 3 HRTEM images of some typical metallic nanoparticles from the specimens: (a) Au, (b) Pt, (c) Co and (d) Cr nanoparticles.

density of the metallic nanoparticles in the pores is relatively low. X-Ray scattering experiments did not give rise to any reflections in the high-angle region indicating that the deposits are either amorphous or too small to give rise to diffraction. Similar observations were made for the Pt-containing material (Fig. S5† – small particles within single pores). Only low loading (1.6 wt%) of Pt was achieved by this synthetic approach due to the limited solubililty of the metal precursor in the methanol evolved during the hydrolysis of TMOS.

For the materials obtained from EDTA complexes, it is only when the specimen is very thin that some nanoparticles inside the channels become just visible (Fig. 2c). When some channels accommodate relatively more metal particles, the image contrast of the corresponding spots against the wall may be reduced. The appearance of this phenomenon can also be observed when the TEM image is taken with an over-focus condition as shown in Fig. 2d, where the channels are imaged as black disks. Two of these disks indicated by the arrows (top) almost lose their darkness due to a large occupancy of the Fe particles. Another arrow in the lower part of Fig. 2d shows a dumbbell pattern and the neighbouring wall is distorted heavily, indicating the possible presence of metal particles that are much larger than the pore diameter. Although it is difficult to see the nanoparticles directly, energy dispersive X-ray microanalysis (EDX) showed that metals had been embedded in all mesoporous silicate particles. Typical EDX spectra, along with further TEM images of Fe and Co systems, are shown in Fig. S6–S8.†

The morphologies and detailed crystal structures of the metal nanoparticles in the mesoporous silicates were revealed by high resolution TEM (HRTEM) (Fig. 3). All the measured *d*-spacings and interplane angles from the nanocrystallites indicate that they are cubic metal structures. Thus, the *d*-spacings of 0.21 nm along the [100] direction matches that of the (200) planes of the cubic Au phase (Fig. 3a), while the fringes in Fig. 3(b) give a *d*-spacing of 0.23 nm, corresponding to the (111) planes of cubic Pt. Similarly Fig. 3c shows a two-dimensional lattice when viewed down the [110] zone axis of the face-centred cubic Co phase with $a = 0.36$ nm and Fig. 3d shows a relatively large particle of Cr recorded along the [100] direction of the cubic phase of Cr with the unit cell parameter $a = 0.46$ nm. Images for Pd, Au and Fe samples are in Fig. S9–S11.†

Curiously, the samples obtained for iron appeared rust-coloured and XPS analysis showed the presence of Fe_3O_4, while for chromium, XPS showed the presence of Cr_2O_3. However, more detailed TEM/HRTEM showed a mixture of larger and smaller iron particles, and spacings and location were consistent with the (smaller) iron metal particles being enclosed within the pores, while the (larger) iron oxide particles were outside of the pores. Representative HRTEM data are given in the ESI (see Fig. S12†).

It is interesting to note that in the case of the Au- and Pd-containing samples the nanoparticles occupy two pore widths, while for the rest the particles are smaller and do not extend beyond one pore (the particle in Fig. 3d appears on the surface and is atypical of the bulk). We believe that this is related to the stability of the metal source, so that the chlorometallates of Pd and Au decompose fairly readily under the conditions of calcination, while the other salts are more stable. Thus, in these latter cases, there is more time for the pores to form and so they are able to contain the metal particles formed, so limiting their size. This is consistent with the behaviour of the Ru–bipyridine complexes, which are quite thermally stable and where only small particles are observed.

From this evidence it is clear that a facile, one-step, synthetic approach to metal-containing mesoporous silicates has been developed using simple starting materials available commercially. The morphology of the resulting materials is predictable due to the application of the true liquid crystal templating technique and an even distribution of uniformly sized metal nanoparticles has been achieved.

We thank EPSRC for support (NCK), Johnson Matthey for generous loans of precious metal salts and Drs Jillian Bailie (Johnson Matthey) and Karen Wilson (York) for XPS data.

Notes and references

1 J. S. Beck, J. C. Vartuli, W. J. Roth, M. E. Leonowicz, C. T. Kresge, K. D. Schmitt, C. T.-W. Chu, D. H. Olsen, E. W. Sheppard, S. B. McCullen, J. B. Higgins and J. L. Schlenker, *J. Am. Chem. Soc.*, 1992, **114**, 10834.
2 See *e.g.*: D. S. Shephard, T. Maschmeyer, G. Sankar, J. M. Thomas, D. Ozkaya, B. F. G. Johnson, R. Raja, R. D. Oldroyd and R. G. Bell, *Chem.–Eur. J.*, 1998, **4**, 1214.
3 G. S. Attard, J. C. Glyde and C. G. Göltner, *Nature*, 1995, **378**, 366.
4 D. W. Bruce, J. D. Holbrey, A. R. Tajbakhsh and G. J. T. Tiddy, *J. Mater. Chem.*, 1993, **3**, 905.
5 J. Bowers, M. J. Danks, D. W. Bruce and R. K. Heenan, *Langmuir*, 2003, **19**, 292; J. Bowers, M. J. Danks, D. W. Bruce and J. R. P. Webster, *Langmuir*, 2003, **19**, 299; J. Bowers, K. E. Amos, D. W. Bruce and J. R. P. Webster, *Langmuir*, 2005, **21**, 1346; J. Bowers, K. E. Amos, D. W. Bruce and R. K. Heenan, *Langmuir*, 2005, **21**, 5696.
6 H. B. Jervis, M. Raimondi, R. Raja, T. Maschmeyer, J. M. Seddon and D. W. Bruce, *Chem. Commun.*, 1999, 2031.
7 N. C. King, C. Dickson, W. Zhou and D. W. Bruce, *Dalton Trans.*, 2005, 1047.
8 M. J. Danks, H. B. Jervis, M. Nowotny, W. Zhou, T. A. Maschmeyer and D. W. Bruce, *Catal. Lett.*, 2002, **82**, 95.
9 O. Dag, S. Alayoglu and I. Uysal, *J. Phys. Chem. B*, 2004, **108**, 8439; A. F. Demirors, B. E. Eser and O. Dag, *Langmuir*, 2005, **21**, 4156.
10 O. Dag, O. Samarskaya, N. Coombs and G. A. Ozin, *J. Mater. Chem.*, 2003, **13**, 328.
11 V. Hulea, D. Brunel, A. Galarneau, K. Philippot, B. Chaudret, P. J. Kooyman and F. Fajula, *Microporous Mesoporous Mater.*, 2005, **79**, 185.
12 C. J. Brinker and G. W. Scherer, *Sol-Gel Science, The Physics and Chemistry of Sol-Gel Processing*, Academic, San Diego, 1990.